mainly observed in the case of strained cycles like cyclopropanes, in the course of stoichiometric reactions [R. A. Periana and R. G. Bergman, *J. Am. Chem. Soc.* **106**, 7272 (1984); R. H. Crabtree, *Chem. Rev.* **85**, 245 (1985); R. J. Puddephatt, *Coord. Chem. Rev.* **33**, 149 (1980)]. It has also been observed with an unstrained C–C bond where the resulting formation of a cyclopentadienyl ligand could be the driving force [R. H. Crabtree and R. P. Dion, *J. Chem. Soc. Chem. Commun.* **1984**, 1260 (1984)]. The oxidative addition of strained cycles has also been assumed in the course of catalytic processes involving the insertion of olefins [H. Takaya, T. Suzuki, Y. Kumagai, M. Yamakawa, R. Noyori, *J. Org. Chem.* **46**, 2846 (1981); H. Takaya *et al., ibid.,* p. 2854].
17. M. E. Thompson *et al., J. Am. Chem. Soc.* **109**, 203 (1987); P. L. Watson, *ibid.* **105**, 6491 (1983).
18. H. G. Woo, J. F. Walzer, T. D. Tilley, *ibid.* **114**, 7047 (1992).

17 December 1996; accepted 6 February 1997

# Thermal Structure of Jupiter's Upper Atmosphere Derived from the Galileo Probe

Alvin Seiff,* Donn B. Kirk, Tony C. D. Knight, Leslie A. Young, Frank S. Milos, Ethiraj Venkatapathy, John D. Mihalov, Robert C. Blanchard, Richard E. Young, Gerald Schubert

**Temperatures in Jupiter's atmosphere derived from Galileo Probe deceleration data increase from 109 kelvin at the 175-millibar level to 900 ± 40 kelvin at 1 nanobar, consistent with Voyager remote sensing data. Wavelike oscillations are present at all levels. Vertical wavelengths are 10 to 25 kilometers in the deep isothermal layer, which extends from 12 to 0.003 millibars. Above the 0.003-millibar level, only 90- to 270-kilometer vertical wavelengths survive, suggesting dissipation of wave energy as the probable source of upper atmosphere heating.**

The exospheric temperature of Jupiter's upper atmosphere as determined by Voyager solar occultation was 1100 ± 200 K at 1400 km above the 1 bar level (*1*). This is much hotter than expected based on Jupiter's remoteness from the sun (*2*). In subsequent fly-by's, Voyager occultations found hot exospheres at the other giant planets (*3–5*), suggesting that common, non-solar mechanisms were acting to heat giant planet exospheres. Three mechanisms have been proposed: (i) heating by collisions of energetic particles with the neutral upper atmosphere (*6*), (ii) heating by dissipation of upward propagating gravity waves (*7*, *8*), and (iii) Joule heating by currents in the ionosphere (*9*). Further progress toward understanding the heating mechanism(s) has been hampered by the lack of a well-characterized temperature profile (*8*).

A. Seiff, Department of Meteorology, San Jose State University Foundation and MS 245-1, Ames Research Center, Moffett Field, CA 94035, USA.
D. B. Kirk, University of Oregon, 37465 Riverside Drive, Pleasant Hill, Oregon 97455, USA.
T. C. D. Knight, 2370 S. Brentwood St., Lakewood, CO 80227, USA.
L. A. Young, Center for Space Physics, Boston University, 725 Commonwealth Ave., Boston, Massachusetts 02215, USA.
F. S. Milos, M.S. 234-1, Ames Research Center, NASA, Moffett Field, CA 94035, USA.
E. Venkatapathy, Eloret Institute, MS 230-2, Ames Research Center, Moffett Field, CA 94035, USA.
J. D. Mihalov and R. E. Young, MS 245-3, Ames Research Center, Moffett Field, CA 94035, USA.
R. C. Blanchard, MS 408A, Langley Research Center, NASA, Hampton, VA 23681, USA.
G. Schubert, Department of Earth and Space Sciences, University of California, Los Angeles, CA 90024, USA.

*To whom correspondence should be addressed. E-mail: aseiff@mail.arc.nasa.gov

Early analysis of the Galileo probe entry data indicated a jovian exospheric temperature of 1350 K at 800 km altitude, essentially confirming the occultation result (*10*). Long vertical wavelength oscillations in the temperature profile suggested gravity waves. This analysis assumed that the atmospheric composition did not vary with altitude, the heat shield ablation mass loss was defined by pre-encounter calculations, first-approximation aerodynamics, zero-readings (offsets) of the acceleration sensors on the most sensitive range were unchanged after pre-entry calibration, and a pressure at 1000 km of 2.2 nbar, equivalent to a threshold temperature of 1150 K. Here, we explore the effect of initial pressure, refine the approximations, and revise the profile of Jupiter's middle and upper atmosphere, starting just below the temperature minimum near 175 mb, the tropopause. We also show the development of wavelike oscillations in the temperature structure above the tropopause.

The probe entered the atmosphere at the edge of a 5-μm hot spot (*11*) in a near-easterly direction (that is, aligned with planetary rotation) at a relative velocity of 47.4054 km/s along a descending flight path at an angle 8.4104° below horizontal (*12*). Data acquisition began at 1028 km, where the deduced pressure was ~1 nanobar and the molecular mean free path was ~0.5 km. This placed the probe deep in the rare gas or free-molecular flow regime. The transition from free-molecular to continuum flow was between ~400 and 300 km altitude. Drag coefficients in rare gas and continuum flow regimes were determined within ~1% by ballistic range tests of scale models and by computational fluid dynamics analysis prior to encounter (*13*). Probe deceleration was measured over a dynamic range of $10^7$ by multi-range accelerometers (*14*), with uncertainties in sensor scale factor ~0.01% and, in offset (zero reading), ~1 count. Data obtained from two independent sensors agreed within ~1 count. We have corrected the data for drift in the offset on the most sensitive range based on data taken during a cruise (in-flight) mission simulation test in November 1992. The initial $z_1$ offset was increased by 5.7 counts, with 1 count uncertainty. The resulting $17 \times 10^{-6}$ *g* correction is important near measurement threshold.

During entry, the probe heat shield was ablated by radiative and convective heating from the shock-layer plasma, which calculations indicate attained a temperature of ~16,000 K near the 5 mb level (*15*). Sensors embedded in the heat shield measured the surface recession as a function of time, and were used to calculate changes in probe mass and frontal area as functions of time (*16*). About one-fourth of the probe mass (90.2 ± 5.8 kg of carbon) was vaporized and/or spalled from the heat shield surface. Variations in probe mass occurred in the late stages of the entry, between 150 km and 80 km altitude, but minor pyrolitic vapor loss occurred after that and was included in the probe mass model. The uncertainty in the mass loss, ±7%, left a formal uncertainty of ±2.3% in the residual probe mass, and hence in the atmospheric density below ~100 km altitude. At the start of descent, density calculated from pressure and temperature measurements agreed closely with the final density from the entry profile, demonstrating small density uncertainty.

The density of the atmosphere was derived from probe decelerations through Newton's second law and the defining equation for drag coefficient,

$$D = (1/2)(\rho V^2)C_D A = ma \qquad (1)$$

Here, $D$ is the aerodynamic drag on the probe; $\rho$, the atmosphere density; $V$, the probe velocity; $C_D$, its drag coefficient; $A$, the frontal area, $m$, the probe mass; and $a$, the deceleration. Probe velocity was determined as a function of time by integrating the measured probe decelerations. Altitudes above the start of descent were determined by integrating the vertical component of

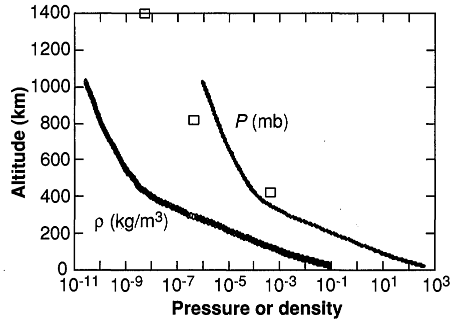


**Fig. 1.** Densities measured and pressures derived from the density data. Threshold density was 3 x $10^{-11}$ kg/m$^3$; pressures extend from 1 nanobar to 400 mb. Pressures are compared with Voyager occultation results (squares) (*5*).

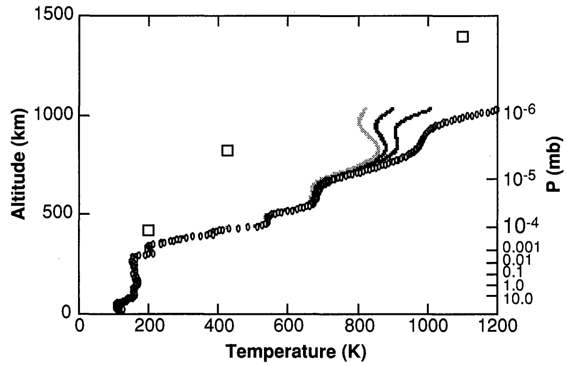


**Fig. 2.** Temperatures given by data in Fig. 1 and the equation of state (circles). The four profiles which assume upper boundary temperatures from 800 to 1200 K converge to within ±15 K at 700 km. Voyager solar and stellar occultation results are shown as squares (*5*). The exospheric temperature from solar occultation and the point at 400 km altitude agree with the present sounding, but the temperature derived from hydrogen absorption of UV starlight at 800 km differs from the present results by >400 K.

velocity over time, for which path angle relative to a horizontal plane is needed. Time histories were obtained by reconstructing the probe trajectory by use of the equations of motion, the measured accelerations, and knowledge of planetary gravity and radius (23.237 m/s$^2$ and 71350 km at the entry site 1-bar level), and rotation rate (0.00017585 rad/sec). The derived density profile and pressures obtained from the density profile with the assumption of hydrostatic equilibrium are shown in Fig. 1. An initial pressure of 0.95 nanobars was assumed, corresponding to an initial temperature of 900 K at 1027 km. For exosphere temperatures from 800 to 1200 K, pressure at the experiment threshold varies from 0.9 to 1.3 nanobars. Voyager solar and stellar occultation pressures differ from the pressure profile by up to a factor of 10 (Fig. 1).

Temperatures were derived from these pressures and densities and the equation of state, $P = \rho RT$ (Fig. 2) for threshold temperatures from 800 to 1200 K. The gas constant, $R$, varies with altitude according to a composition model, which defines atmospheric mean molecular weight as a function of altitude (*17*). The uncertainty arising from the undefined initial temperature at measurement threshold subsides rapidly within the first decade of pressure increase. The present sounding is consistent with the Voyager solar occultation exospheric temperature measurements at 1400 km altitude, considering its uncertainty in temperature (±200K) and altitude (±200 km) (Fig. 1). The point at 830 km, inferred from stellar ultraviolet (UV) absorption by hydrogen, is, however, 400 K below the in situ profile.

The isothermal layer at $T \sim 160$ K, which extends from 12 to 0.003 mb (80 to 300 km) (Fig. 2) suggests efficient mixing, with warming supplied by downward heat conduction from above 300 km. Temperature oscillations with altitude occur throughout the sounding. Within and below the isothermal layer, vertical wavelengths are short, 10 to 50 km. Above 300 km, they are much longer, 90 to 280 km. The shorter waves may be damped at low altitudes by breaking, while the longer waves with lower temperature gradients do not break, but instead, persist upward. Such filtering removes shorter waves, leaving the long waves to warm the upper atmosphere. Gravity waves may explain the upper atmospheric warming (*7*, *8*, *18*).

Near 300 km (Fig. 2), there is a feature with a steep lower edge and an overshoot at its peak. This could be a short wavelength peak at the start of the upper region heating, or it may be an artifact, since the drag coefficient may not have been modeled exactly in this region where the flow changes from free-molecular to continuum. Moving upward from 300 km, there is a hitch in the curve at 355 km, a weak temperature plateau at 400 km, and other plateaus with progressively increasing amplitudes starting at 460, 550 km, and 820 km. From these inflections, estimated vertical wavelengths are 50, 60, 90, and 270 km. This nonuniform stucture suggests the presence of more than a single wave. Amplitude growth with decreasing density is observed, as is expected if these oscillations are caused by gravity waves.

The mean temperature gradient is uncertain above 800 km. Where heat deposition ceases, the temperature gradient at equilibrium must go to zero so that there is no heat loss downward, or more heat loss upward than can be radiated to space. Approach to an isothermal state above 800 km is suggested with initial temperatures of 800 to 1000 K, although wavelike inflection in these profiles suggests continuing wave propagation. In Seiff *et al.* (*10*), temperatures decrease upward above 800 km, implying upward conduction of heat to an unknown sink. Here we excluded initial temperatures <800 K that would indicate strong upward conduction.

The tropopause, the level at which lower atmospheric mixing ceases, is characterized by a temperature minimum. It was encountered during late stages of probe entry rather than after the start of descent on the parachute, as planned (*19*). In general, the remote sensing measurements of the Voyager Infrared Interferometer Spectrometer (IRIS) (*20*) agree with the probe sounding (Fig. 3). The exact location of the tropopause is somewhat obscured in the higher resolution data by probe buffeting at subsonic speeds and by temperature oscillations. The latter appear immediately at altitudes above (pressures below) the temperature minimum, where the atmosphere becomes statically stable, and they grow in amplitude with decreasing density, as is characteristic of gravity waves. The near-adiabatic lower atmosphere terminates at pressures just above 175 mb (altitudes below 35 km) at the 109 K temperature minimum. This is identified as the tropopause. The Voyager IRIS tropopause was at 104 K and 150 mb at 10°N in the North Equatorial Belt (NEB). The IRIS profile is smooth and perturbation-free because of profile averaging and relatively coarse altitude resolution. Broad smoothing of the ASI data would likewise tend to lower the tropopause pressure. Thermal structure differences are also probable between a 5-mm hot spot, where the probe descended, and the mean state of the NEB. These observations provide a basis for improved analysis of the processes controlling the structure of the middle and upper atmosphere of Jupiter.

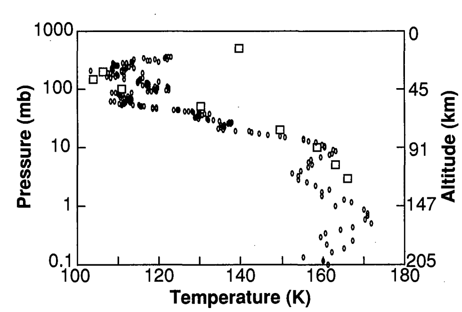


**Fig. 3.** The tropopause region of the ASI sounding results (expanded from Fig. 2) (circles) compared with the Voyager IRIS results (squares).

Hot exospheres seen in other giant planetary atmospheres are likely produced by mechanisms similar to those on Jupiter.

## REFERENCES AND NOTES


1. M. C. Festou *et al.*, *J. Geophys. Res.* **86**, 5715 (1981).
2. D. F. Strobel and G. R. Smith, *J. Atm. Sci.* **30**, 718 (1973).
3. G. R. Smith *et al.*, *J. Geophys. Res.* **88**, 8667 (1983).
4. F. Herbert *et al.*, *ibid.* **83**, 15093 (1987).
5. A. L. Broadfoot *et al.*, *Science* **246**, 1459 (1989).
6. D. M. Hunten and A. J. Dessler, *Planet. Space Sci.* **25**, 817 (1977).
7. S. K. Atreya *et al.*, *Geophys. Res. Lett.* **6**, 10795 (1979).
8. R. V. Yelle *et al.*, *J. Geophys. Res.* **101**, 2149 (1996).
9. A. Nishida and Y. Watanabe, *ibid.* **86** (no. A12), 9945 (1981); S. K. Atreya, T. M. Donahue, and M. C. Festou, *Astrophys. J.* **247**, L43 (1981).
10. A. Seiff *et al.*, *Science* **272**, 844 (1996). All altitudes in this paper refer to the 1-bar level.
11. G. Orton *et al.*, *ibid.*, p. 839.
12. Personal communication from J. Neff. These parameters are for an altitude of 450 km, the probe entry altitude as defined by the Probe Project Office. They were derived from radio tracking of the orbiter, measurement of the probe separation impulse, the equations of motion, and a model of Jupiter's gravity field. Latitude and longitude at the entry altitude were 6.5303°N and 4.9403°W in System III coordinates, with heading angle 92.6111° clockwise from north. We extended this trajectory upward to the altitude of first data acquisition, where relative velocity and path angle were 47.1303 km/s and 10.6218°, respectively.
13. A. Seiff, E. Venkatapathy, B. Haas, P. Intrieri, *AIAA-96-2451*, 14th AIAA Applied Aerodynamics Conference, New Orleans, LA, 17 to 20 June 1996.
14. Sensors were Bell Model XI guidance accelerometers. To preserve precision over a wide dynamic range, four measurement ranges were implemented with 12-bit digital resolution [A. Seiff and T. C. D. Knight, *Space Sci. Rev.* **60**, 203 (1992)]. Resolution was $3.1 \times 10^{-6}$ *g* on the most sensitive range; 0.1 *g* on the least sensitive. The first data point retained in memory was $2.057 \times 10^{-4}$ m/s$^2$ or $21 \times 10^{-6}$ *g*. Peak deceleration was 2240 m/s$^2$ (228 *g*), at an altitude of 101 km above the 1 bar level. (*g* denotes Earth sea-level acceleration of gravity, 9.80665 m/s$^2$.) An excellent data set was realized, exceeding in both accuracy and altitude and measurement resolution those from a similar experiment at Venus [A. Seiff and D. B. Kirk, *J. Geophys. Res.* **96**, 11,021 (1991); *Icarus* **49**, 45 (1982)].
15. J. N. Moss and A. L. Simmonds, in *Progress in Astronautics and Aeronautics* , P. E. Bauer and H. E. Collicott, Eds. (AIAA, New York, 1983), pp. 419-445.
16. F. S. Milos, *AIAA-96-1823*, 31st AIAA Thermophysics Conference, New Orleans, LA, 17 to 20 June 1996.
17. Below the homopause, composition was based on measurements in the lower atmosphere by the neutral mass spectrometer [H. B. Niemann *et al.*, *Science* **272**, 846 (1996)] and the helium abundance detector (U. von Zahn *et al.*, *ibid.*, p. 849). Above the clouds, where $H_2O$ and $NH_3$ have been removed by condensation, we selected 0.8625, 0.1358, and 0.0017 for the mole fractions of $H_2$, He, and $CH_4$. The homopause, formally, the altitude of equal turbulent and molecular diffusion, is at 370 km. Above the homopause, we calculate the composition assuming diffusive equilibrium [S. K. Atreya, *Atmospheres and Ionospheres of the Outer Planets and Their Satellites* (Springer-Verlag, New York, 1986), p. 89] with a turbulent diffusion coefficient of $5 \times 10^6$ cm$^2$/s [R. J. Vervack *et al.*, *Icarus* **114**, 163 (1995)]. Heavy constituent mole fractions are reduced by diffusive separation to 0.028 (He) and $7 \times 10^{-7}$ ($CH_4$) at 500 km, and essentially vanish at 1000 km, while atomic H rises to 0.031 at 1000 km. The gas constant varies from 2.35 J/kg K below the homopause to 1.99 J/kg K at 1000 km.
18. L. A. Young, R. V. Yelle, R. E. Young, A. Seiff, and D. B. Kirk, *Science* **276**, 108 (1997).
19. This resulted from 53 s late deployment of the probe parachute [R. E. Young, M. A. Smith, C. K. Sobeck, *ibid.* **272**, 837 (1996)].
20. R. Hanel *et al.*, *ibid.* **204**, 972 (1979); V. Kunde *et al.*, *Astrophys. J.* **263**, 443 (1982).



22 January 1997; accepted 14 March 1997


# Equatorial X-ray Emissions: Implications for Jupiter's High Exospheric Temperatures


J. H. Waite Jr.,* G. R. Gladstone, W. S. Lewis, P. Drossart, T. E. Cravens, A. N. Maurellis, B. H. Mauk, S. Miller



**Observations with the High Resolution Imager on the Röntgensatellit reveal x-ray emissions from Jupiter's equatorial latitudes. The observed emissions probably result from the precipitation of energetic (>300 kiloelectron volts per atomic mass unit) sulfur and oxygen ions out of Jupiter's inner radiation belt. Model calculations of the energy deposition by such heavy ion precipitation and of the resulting atmospheric heating rates indicate that this energy source can contribute to the high exospheric temperatures (>800 kelvin at 0.01 microbar) measured by the Galileo probe's Atmospheric Structure Instrument. Low-latitude energetic particle precipitation must therefore be considered, in addition to other proposed mechanisms such as gravity waves and soft electron precipitation, as an important source of heat for Jupiter's thermosphere.**


X-rays from Jupiter's northern and southern auroral zones are believed to be line emissions from precipitating sulfur and oxygen ions (*1–4*). Observations made in July 1994 with the High Resolution Imager (HRI) on board the Earth-orbiting Röntgensatellit (ROSAT) reveal, in addition to the expected high-latitude auroral emissions (*5*), well-defined emissions emanating from near Jupiter's equator (*6*), suggesting that energetic ion precipitation occurs at low as well as high latitudes. Charged particle precipitation in the auroral zones, together with Joule heating, is thought to play a major—and perhaps the dominant—role in the global energetics and dynamics of Jupiter's upper atmosphere (*7–9*). Energetic ion precipitation at lower latitudes would thus be expected to have aeronomical effects and must be considered, along with soft electron precipitation at middle and low latitudes (*10*) and breaking gravity waves (*11*), as a possible thermospheric energy source. Such heating mechanisms must be invoked to account for thermospheric temperatures that are much higher than can be explained solely in terms of solar extreme ultraviolet (EUV) heating of Jupiter's upper atmosphere (*12*). Here, we analyze Jupiter's equatorial x-ray emissions, which we assume are excited by precipitating sulfur and oxygen ions, and present calculations of the effects of such energetic ion precipitation on the thermal structure of the jovian equatorial thermosphere.

We observed Jupiter with the ROSAT HRI in July 1994, shortly before and during the impact of comet Shoemaker-Levy 9 (*13*). Although x-ray emissions from Jupiter's equatorial and auroral regions were detected before and during the impact period, we consider for this study only the preimpact data to avoid biasing the analysis by including any unique events associated with the impacts.

Low-latitude x-ray emissions (like those at higher latitudes) are organized in solar local time, occurring predominantly between local noon and dusk in these data (Fig. 1A). Local time organization of the equatorial and auroral x-ray emissions is also evident in HRI observations from March and September 1996. Like the July 1994 observations, the September 1996 observations show that the x-rays emanate principally from the planet's noon-dusk sector. In the case of the March observations, however, the emissions occur preferentially in the morning, rather than the afternoon, sector. The reasons for the local time organization of the jovian x-ray emissions and for the variation between morning and afternoon sectors are not currently understood.

In addition to their organization in local


J. H. Waite Jr., G. R. Gladstone, W. S. Lewis, Department of Space Science, Southwest Research Institute, Post Office Box 28510, San Antonio, TX 78228–0510, USA.
P. Drossart, DESPA, Observatoire de Paris, F-92195 Meudon Cedex, France.
T. E. Cravens and A. N. Maurellis, Department of Physics and Astronomy, University of Kansas, Lawrence, KS 66045–2151, USA.
B. H. Mauk, Applied Physics Laboratory, The Johns Hopkins University, Laurel, MD 20723–6099, USA.
S. Miller, Department of History, Philosophy, and Communication in Science, University College London, London WC1E 6BT, UK.

*To whom correspondence should be addressed. E-mail: hunter@kronos.space.swri.edu